Neuroradiology (2004) 46: 258–266
DOI 10.1007/s00234-003-1154-2



**J. F. L. Schneider**
**K. A. Il'yasov**
**J. Hennig**
**E. Martin**

# Fast quantitative diffusion-tensor imaging of cerebral white matter from the neonatal period to adolescence

Received: 6 July 2003
Accepted: 29 November 2003
Published online: 4 March 2004


J. F. L. Schneider (✉) · E. Martin
Department of Neuroradiology
and Magnetic Resonance Imaging,
University Children's Hospital,
Steinwiesstrasse 75, 8032 Zürich,
Switzerland
E-mail: jacques.schneider@kispi.unizh.ch
Tel.: +41-1-2667828
Fax: +41-1-2667153

K. A. Il'yasov · J. Hennig
Department of Diagnostic Radiology,
Section of Medical Physics, University
Medical Centre, Hugstetter Strasse 55,
79106 Freiburg, Germany

**Abstract** We investigated the isotropic diffusion coefficient (D') and fractional anisotropy (FA) in white matter (WM) during brain development, using an optimised diffusion-tensor imaging (DTI) method with whole brain coverage in a clinically acceptable time. We images 52 children with no evident neurological abnormality (30 boys, 22 girls aged 1 day–16 years) using high-angle DTI with optimised temporal gradient performance. D' and FA were calculated in 10 regions of interest in white matter. We saw that the age-related reduction in D' and increase in FA follow a mono- or biexponential model in white matter, probably depending on the compactness and myelination rate of the fibre tracts. In contrast to other areas, in which adult values were reached during the third year, there is a trend to continuous increase in FA in all deep white-matter areas, suggesting continuing maturation and organisation of deep tracts not detected on conventional MRI.

**Keywords** Diffusion-tensor imaging · Brain maturation · White matter

## Introduction

Until recently, conventional MRI allowed visualisation of the myelination of the white matter through signal intensity changes on T1- and T2-weighted images. Assessing myelination is of interest for better diagnosis and understanding of inborn errors of metabolisms, developmental delay and demyelinating diseases. Understanding normal brain water diffusion has served as a template for investigation of neurological diseases. Diffusion-tensor imaging (DTI) characterises the spatial properties of molecular diffusion [1, 2]. Beside cerebral ischaemia, DTI has found applications in a wide range of clinical situations and in developmental studies [3, 4, 5]. Its application to the central nervous system has revealed that diffusion of water in white matter is anisotropic, probably due to the ordered structure of axons and myelin sheaths [6, 7]. The magnitude of diffusion and preferential orientation can be quantified, providing insights into white-matter microstructure.

Imaging of newborns and infants has demonstrated higher apparent diffusion coefficients (ADC) and less anisotropy than in adults [8, 9]. Early changes in ADC and anisotropy (even before changes in signal on T1- and T2- weighted images take place) are supposed to represent changes in premyelination before histological or MRI evidence of myelination and the role of the sodium-channel pump has been emphasised [10, 11, 12]. Later changes during infancy and childhood are attributed to decreasing water content and progression of myelination [13]. Some important diffusion-tensor derived measures, such as indices of diffusion anisotropy, are highly sensitive to the signal-to-noise ratio (SNR) of the input data [14] and signal averaging is therefore usually required. On the other hand, fibre-tracking or "tractography", which aims to reconstruct white matter tracts in three dimensions by following the path of greatest diffusion—the direction which parallels the eigenvector with the largest eigenvalue—depends on accurate estimation of the orientation of the intravoxel tensor. This requires

an optimal SNR and the highest possible spatial resolution but implies very long acquisition times. Full brain coverage with acquisition times between 15 and 40 min have been reported [15, 16]. These very long times restrict the introduction of this technique to clinical routine. Our aim was to elaborate an age-related timetable of changes in the isotropic diffusion coefficient (D') and fractional anisotropy (FA) in the cerebral white matter from normal neonates to adults and for this purpose a diffusion-tensor method was optimised for higher SNR and spatial resolution in a clinically reasonable time.

## Materials and methods

We reviewed children referred for neuroimaging. Inclusion criteria were normal brain imaging including DTI, no signs of neurological dysfunction, no deficits and no developmental delay. Patients with known organic brain disorders were excluded. We studied 52 patients (30 boys, 22 girls, age 1 day–16 years, median 5.5 years, mean 6.6 years) (Table 1). No child was examined more than once. The studies were performed with the approval of the institutional ethics committee.

All MRI was performed at 2.0 tesla, with a 30 mT/m gradient system. Diffusion-weighted imaging (DWI) was performed with a multislice single-shot diffusion-weighted spin-echo echoplanar (EPI) sequence: TR 5900 TE 102 ms, field of view 256×256 $mm^2$, whole brain coverage with 19–30 4 mm contiguous slices, depending on patient size. Raw data size was 128×68 (70% k-space covering). Raw data were corrected for sampling errors (regridding) and reconstructed to 128×128. Diffusion encoding was along 60 directions evenly distributed over a sphere. Diffusion weighting was optimised according to Jones et al. [17], i.e. only one measurement with high diffusion weighting was made for each of the 60 diffusion-encoding gradient directions and six were made with low diffusion weighting; the effective b was approximately 1500 $s/mm^2$.

To optimise the temporal performance of the gradients, the standard EPI sequence was modified as follows. The ramp times of the diffusion-encoding gradients were set to 1 ms, with slew rates within safety values; gradients were positioned asymmetrically around the refocusing radiofrequency pulse to obtain maximal diffusion weighting in the shortest echo time; and we found empirically that by moderately reducing the amplitude of the EPI readout gradients, by setting a minimal field of view at 256 mm, the gradient performance allows multislice DWI with a shorter TE, giving a higher SNR, and a minimal pause between EPI shots of 40 ms; this was a prerequisite for whole-brain coverage in the above mentioned TR. As a result of these improvements, SNR in the raw images was increased by about 50% relative to standard DWI sequences with the same diffusion weighting and was typically around 68 (white matter, b 0 image without averaging) and 20 (b 1500 $s/mm^2$, same location). Total acquisition time was approximately 6.5 min. The images were corrected for eddy current-induced geometrical distortions (magnification, translation and shear) according to the modified procedure of Bastin and Armitage [18]. The b matrix was calculated numerically including all imaging- and diffusion-encoding gradients.

Diffusion tensor components were computed pixel-by-pixel and diagonalised to find the fibre directions, using homemade routines developed on Matlab. Exact calibration of the gradient amplitudes and verification of the quantitative diffusion measurements was on a water-filled phantom. After calibration the coincidence between the diffusion constants measured for different diffusion-encoding directions was in a good agreement with temperature-compensated data for diffusion constants in water [19]. FA maps in the water phantom showed that the anisotropy index was below noise level and around zero.

All maps were reviewed by two radiologists (JFLS and EM). Using homemade software, we obtained D' and FA from the DTI in left and right anatomical regions after placing manually selected ROI in the following white-matter areas: the crus of the pons (Pons); crus cerebri (Crus); posterior limb of internal capsule (PLIC); centrum semiovale (CSO); frontal, parietal, temporal and occipital white matter (FWM, PWM, TWM, OWM); and the genu and splenium of the corpus callosum (GCC, SCC).

D' and FA were derived from the left and right ROI and averaged in each patient. Graphs of D' and FA versus age in all regions were fitted empirically with multiexponential regression, using mono- and biexponential functions. The Levenberg-Marquardt least-squares minimisation was used to determine the best-fit values of the nonlinear model parameters and their standard errors. The decision between bi- and mono-exponential fit was made in a manner similar that described by Mukherjee et al. [20]. The $\chi^2$ values were calculated for the mono-and biexponential regression model and the F-test was used to compare the $\chi^2$ statistics and determine the model which best fits the data.

**Table 1** Age of 52 children studied

| Age (months) | Children |
|---|---|
| 0–2 | 4 |
| 2–4 | 2 |
| 4–12 | 3 |
| 12–24 | 3 |
| 24–36 | 3 |
| 36–48 | 6 |
| 48–96 | 10 |
| 96–144 | 12 |
| >144 | 9 |

## Results

For all ROI, D' was highest in newborns (0–2 months) and lowest in adolescents (>144 months) while FA followed an opposite course, being lowest in newborns and highest in adolescents. We divided white-matter regions into three groups: corticospinal tracts (Pons, Crus, PLIC, CSO), deep white matter (FWM, PWM, OWM, TWM) and corpus callosum (GCC, SCC) (Fig. 1). In all patients, right and left D' and FA of symmetrical ROI showed very good agreement.

In the neonatal period, corticospinal tracts showed the lowest D' of all white matter regions, varying from $0.99\times10^{-3}$ $mm^2/s \pm 0.02$ in Pons to $1.39\times10^{-3}$ $mm^2/s \pm 0.08$ in CSO (Table 2a). There was a continuous decrease in D', best described by a monoexponential regression function for Crus and PLIC. Biexponential regression provided a significant improvement in data fitting for CSO with only low significance for Pons (Table 3a, b). Adult values were reached at 36–48 months.

The four deep white-matter regions showed a parallel time course. All the showed the highest D' at birth (FWM $1.56\times10^{-3}$ $mm^2/s \pm 0.13$, OWM $1.46\times10^{-3}$ $mm^2/s \pm 0.15$).

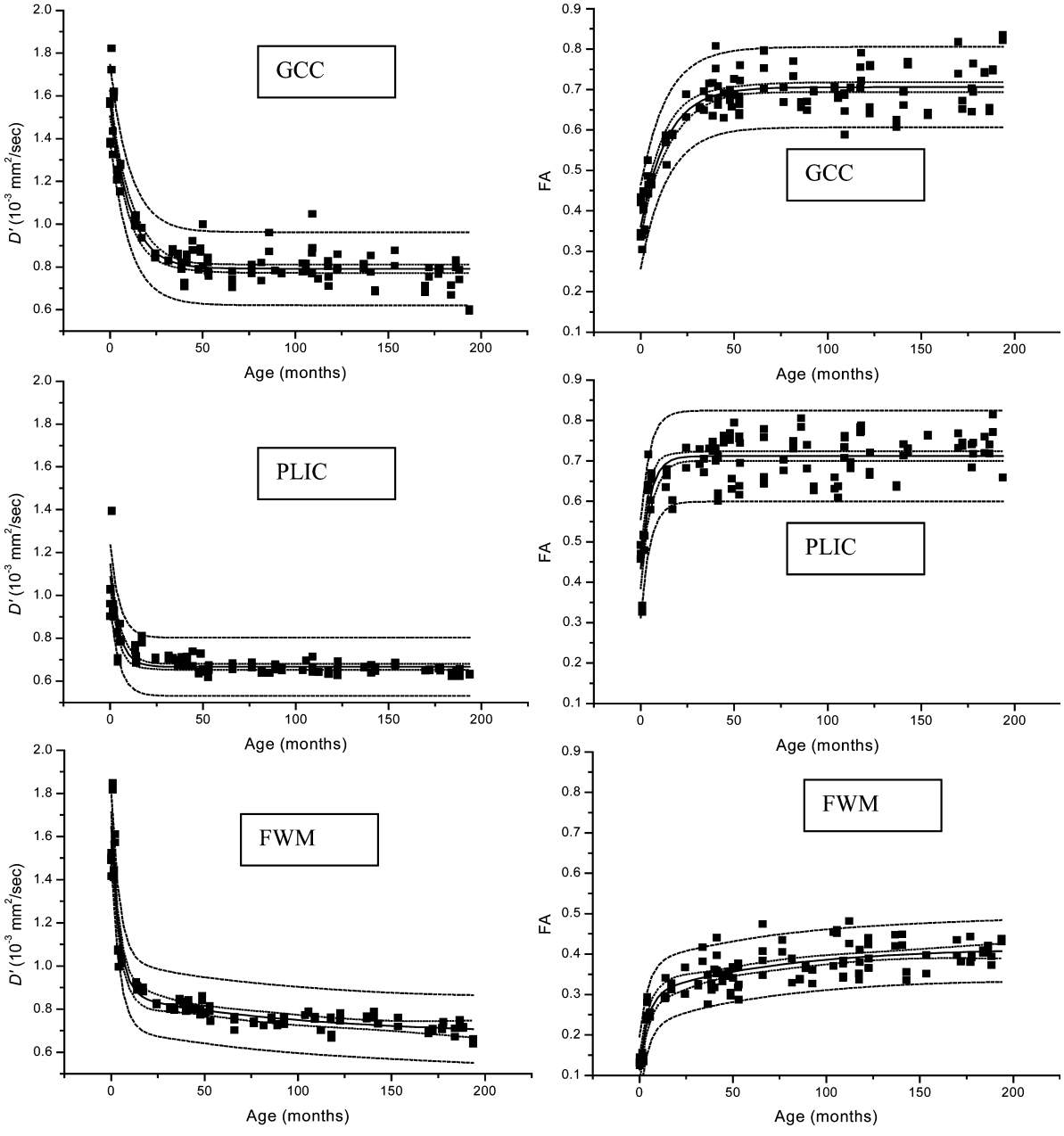


**Fig. 1** Scatter plots showing isotropic diffusion coefficient (D') (*left*) and fractional anisotropy (FA) (*right*) versus age, in the genu of the corpus callosum (*top*), the posterior limb of the internal capsule (*middle*) and frontal white matter (*bottom*). *dotted lines* 95% confidence limits *dashed lines* 95% prediction limits

All four slopes showed a significant improvement in data fitting with a biexponential regression, and adult values were reached slightly earlier than in the corticospinal tract, at 24–36 months. D' time-course values for the GCC and SCC showed parallel slopes best fitted with a monoexponential regression function. Adult values were reached at 24–36 months, showing almost no difference (GCC $0.78\times10^{-3}$ mm$^2$/s $\pm$ 0.20; SCC D' = $0.75\times10^{-3}$ mm$^2$/s $\pm$ 0.18). The GCC showed higher D' than the splenium at all ages (neonatal GCC $1.53^{-3}$ mm$^2$/s $\pm$ 0.21; neonatal SCC $1.44\times10^{-3}$mm$^2$/s $\pm$ 0.24).

The highest neonatal FA was found in the corpus callosum (GCC $0.38 \pm 0.08$; SCC $0.42 \pm 0.07$). Corticospinal tracts showed intermediate values at birth varying from $0.18 \pm 0.01$ (Pons) to $0.45 \pm 0.04$ (PLIC). The lowest neonatal FA was in the deep WM, with values varying from $0.14 \pm 0.04$ (FWM) to $0.20 \pm 0.05$ (TWM) (Table 2b). Highly organised, compact fibre bundles such as Crus and PLIC showed significantly higher values than CSO and Pons. Monoexponential

**Table 2** Isotropic diffusion (D', $10^{-3}$ $mm^2/s \pm s.d$) in white matter as a function of age

| Age (months) | 0–2 | 2–4 | 4–12 | 12–24 | 24–36 | 36–48 | 48–96 | 96–144 | > 144 |
|---|---|---|---|---|---|---|---|---|---|
| Pons | 0.99 (0.02) | 0.81 (0.05) | 0.78 (0.04) | 0.79 (0.06) | 0.64 (0.08) | 0.70 (0.08) | 0.65 (0.08) | 0.62 (0.08) | 0.62 (0.07) |
| Crus | 1.26 (0.11) | 1.08 (0.12) | 0.97 (0.13) | 0.95 (0.12) | 0.84 (0.13) | 0.76 (0.13) | 0.78 (0.11) | 0.73 (0.10) | 0.68 (0.11) |
| Posterior limb internal capsule | 1.07 (0.04) | 0.87 (0.03) | 0.77 (0.04) | 0.75 (0.04) | 0.71 (0.03) | 0.68 (0.03) | 0.66 (0.03) | 0.66 (0.04) | 0.65 (0.04) |
| Centrum semiovale | 1.39 (0.08) | 1.07 (0.05) | 0.94 (0.04) | 0.83 (0.04) | 0.73 (0.03) | 0.72 (0.03) | 0.68 (0.03) | 0.69 (0.03) | 0.64 (0.03) |
| Frontal lobe | 1.56 (0.13) | 1.33 (0.10) | 1.02 (0.07) | 0.90 (0.05) | 0.81 (0.05) | 0.81 (0.05) | 0.76 (0.04) | 0.75 (0.05) | 0.72 (0.05) |
| Parietal lobe | 1.50 (0.12) | 1.38 (0.11) | 1.01 (0.06) | 0.86 (0.06) | 0.80 (0.05) | 0.79 (0.05) | 0.74 (0.05) | 0.73 (0.06) | 0.67 (0.05) |
| Temporal lobe | 1.48 (0.17) | 1.21 (0.12) | 1.05 (0.09) | 0.96 (0.09) | 0.87 (0.12) | 0.88 (0.12) | 0.81 (0.08) | 0.80 (0.09) | 0.78 (0.12) |
| Occipital lobe | 1.46 (0.15) | 1.23 (0.16) | 1.01 (0.14) | 0.89 (0.11) | 0.79 (0.06) | 0.81 (0.09) | 0.75 (0.05) | 0.75 (0.09) | 0.67 (0.10) |
| Genu corpus callosum | 1.53 (0.21) | 1.42 (0.22) | 1.23 (0.27) | 1.00 (0.20) | 0.85 (0.18) | 0.81 (0.17) | 0.83 (0.20) | 0.81 (0.19) | 0.78 (0.20) |
| Splenium corpus callosum | 1.44 (0.24) | 1.21 (0.20) | 1.11 (0.22) | 0.94 (0.24) | 0.78 (0.15) | 0.80 (0.20) | 0.81 (0.20) | 0.75 (0.18) | 0.74 (0.18) |

**Table 3** Statistical comparison between mono- and biexponential fits for D' and FA

| Region | D' | | | | FA | | | |
|---|---|---|---|---|---|---|---|---|
| | $\chi^2$ Monoexponential | $\chi^2$ Biexponential | F(2,N-4) | Best model | $\chi^2$ Monoexponential | $\chi^2$ Biexponential | F(2,N-4) | Best model |
| Pons | 0.0124 | 0.0113 | 5.19[a] | Biexponential | 0.0083 | 0.0082 | 0.58 | Monoexponential |
| Crus | 0.0145 | 0.0140 | 1.66 | Monoexponential | 0.0060 | 0.0047 | 14.35[a] | Biexponential |
| Posterior limb internal capsule | 0.0047 | 0.0044 | 2.75 | Monoexponential | 0.0032 | 0.0031 | 1.19 | Monoexponential |
| Centrum semiovale | 0.0056 | 0.0045 | 12.48[a] | Biexponential | 0.0024 | 0.0022 | 4.99[a] | Biexponential |
| Frontal lobe | 0.0070 | 0.0059 | 10.22[a] | Biexponential | 0.0017 | 0.0014 | 12.11[a] | Biexponential |
| Parietal lobe | 0.0090 | 0.0080 | 7.00 | Biexponential | 0.0031 | 0.0028 | 6.64[a] | Biexponential |
| Temporal lobe | 0.0067 | 0.0053 | 14.54[a] | Biexponential | 0.0024 | 0.0023 | 1.59 | Monoexponential |
| Occipital lobe | 0.0050 | 0.0036 | 20.23[a] | Biexponential | 0.0038 | 0.0036 | 2.78 | Monoexponential |
| Genu corpus callosum | 0.0073 | 0.0070 | 2.81 | Monoexponential | 0.0025 | 0.0025 | −1.04 | Monoexponential |
| Splenium corpus callosum | 0.0088 | 0.0084 | 2.45 | Monoexponential | 0.0031 | 0.0031 | 1.39 | Monoexponential |

[a]statistically significant improvement of the fits (with values above $F(2,106) = 3.08$) which favours a biexponential over a monoexponential model

regression function provided the best fit for GCC and SCC and for TWM, OWM, while biexponential regression was the best fit for FWM, PWM, Crus, CSO (low significance) and Pons (Table 3a, b). Adult values for the GCC and SCC were reached at 24–36 months with slightly higher values in the SCC ($0.76 \pm 0.1$) than in the GCC ($0.70 \pm 0.12$). FA in SCC was higher than in GCC at all ages. In all deep white-matter areas (Fig. 1), a small but continued late increase in anisotropy was seen with maximal FA $0.45 \pm 0.1$ for PWM, OWM and TWM in the oldest patients (12–16 years). FA in FWM was constantly lower than in the other three deep white-matter areas with a less pronounced increase in the final age band.

## Discussion

Diagnostic MRI has to be performed in a limited time and therefore previously reported DTI studies lasting 45 min or more are not suitable for clinical applications. We present a DTI sequence that has been optimised in order to get accurate estimation of diffusion parameters in a reasonable time. Echoplanar DWI is fast and allows whole brain coverage. There is an increasing need for high-quality EPI, especially should white-matter tract reconstruction be needed, implying thinner ( $\leq 4$ mm) slices and eddy-current correction. We made DT measurements along 60 directions instead of averaging measurements along the minimum six diffusion directions, increasing the accuracy of the orientation estimation of the DT and leading to a better estimation of diffusion anisotropy [17]. We assumed monoexponential diffusion decay and therefore only a single high b along each direction was measured. Accurate DT analysis should include correction of the image distortions due to residual eddy currents, which arise from switching of gradients. Modern methods of hard- and software compensation are very effective and eddy-current effects do not usually play a role. However, EPI is very sensitive to all magnetic field inhomogeneity and therefore even very low eddy currents cause significant (up to several pixels) shift, shear and scaling of EPI images along the phase-encoding direction [21, 22]. Variable eddy currents arise from different diffusion-encoding gradients causing variable distortions of EPI. This typically produces a high-signal halo on DTI. On the other hand, such distortions cause blurring of all DTI parametric maps and result in faulty estimation of D' and FA. We chose the FA index, as it maps diffusion anisotropy with the greatest detail and highest SNR [23]. Our data compare favourably with previously published data on DTI of the white matter in childhood [5, 9, 13, 20, 24, 25]. However, these studies were based on indirect DT and anisotropy estimation, making direct comparison with our results difficult (Table 4).

**Table 4** Nonlinear regression parameters for age dependence of D' and FA, fitted to y0 + A1exp(-ageinmonths/t1) + A2exp(-ageinmonths/t2)]

| Region | Parameter | D' fit | FA fit |
|---|---|---|---|
| Pons | Y0 | 0.53 (0.29) | 0.51 (0.03) |
| | A1 | 0.30 (0.07) | −0.28 (0.03) |
| | t1 | 2.31 (1.23) | 60.96 (18.25) |
| | A2 | 0.23 (0.25) | Not applicable |
| | t2 | 181.30 (385.40) | Not applicable |
| Crus | Y0 | 0.75 (0.02) | 0.83 (0.10) |
| | A1 | 0.43 (0.04) | −0.30 (0.05) |
| | t1 | 19.65 (4.47) | 3.32 (1.09) |
| | A2 | Not applicable | −0.28 (0.08) |
| | t2 | Not applicable | 130.48(101.45) |
| Posterior limb internal capsule | Y0 | 0.67 (0.01) | 0.71 (0.01) |
| | A1 | 0.43 (0.03) | −0.28 (0.03) |
| | t1 | 4.97 (0.86) | 5.08 (1.10) |
| Centrum semiovale | Y0 | 0.65 (0.02) | 0.53 (0.01) |
| | A1 | 0.64 (0.06) | –0.16 (0.05) |
| | t1 | 3.32 (0.64) | *2.50 (1.55)* |
| | A2 | 0.20 (0.05) | −0.19 (0.05) |
| | t2 | 42.41 (19.25) | 28.73 (8.82) |
| Frontal white matter | Y0 | 0.68 (0.07) | 0.42 (0.02) |
| | A1 | 0.79 (0.06) | −0.19 (0.03) |
| | t1 | 4.33 (0.64) | 4.35 (1.40) |
| | A2 | 0.19 (0.05) | −0.12 (0.02) |
| | t2 | 97.40 (96.28) | 72.86 (44.05) |
| Parietal white matter | Y0 | 0.66 (0.07) | 0.66 (0.51) |
| | A1 | 0.76 (0.07) | −0.20 (0.03) |
| | t1 | 5.26 (1.00) | 6.12 (2.33) |
| | A2 | 0.17 (0.05) | −0.32 (0.48) |
| | t2 | 87.53 (104.21) | 317.90 (706.96) |
| Temporal white matter | Y0 | 0.76 (0.02) | 0.47 (0.01) |
| | A1 | 0.56 (0.07) | −0.25 (0.01) |
| | t1 | 3.58 (0.82) | 31.47 (4.65) |
| | A2 | 0.22 (0.06) | Not applicable |
| | t2 | 46.57 (21.64) | Not applicable |
| Occipital white matter | Y0 | 0.56 (0.30) | 0.47 (0.01) |
| | A1 | 0.70 (0.04) | −0.25 (0.02) |
| | t1 | 4.44 (0.53) | 37.88 (7.04) |
| | A2 | 0.29 (0.27) | Not applicable |
| | t2 | 235.73 (377.24) | Not applicable |
| Genu of corpus callosum | Y0 | 0.79 (0.01) | 0.71 (0.01) |
| | A1 | 0.78 (0.03) | −0.35 (0.02) |
| | t1 | 10.56 (1.19) | 14.02 (1.90) |
| Splenium of corpus callosum | Y0 | 0.77 (0.01) | 0.74 (0.01) |
| | A1 | 0.69 (0.04) | −0.35 (0.02) |
| | t1 | 9.06 (1.31) | 8.33 (1.41) |

Not applicable: monoexponential fit statistically favoured

The difference between anisotropic and isotropic diffusion can be used to highlight white-matter tracts, assess their integrity and monitor the development of the normal brain. Previous studies performed in preterm and term newborns have shown that, as the brain matures, there is a gradual decline in the mean diffusion and an increase in anisotropy in the white matter, believed to be largely related to the process of myelination [4, 9, 25]. During the laying down of the myelin sheath, water is extruded from the extracellular space resulting in a relative increase in the fraction of intracellular water.

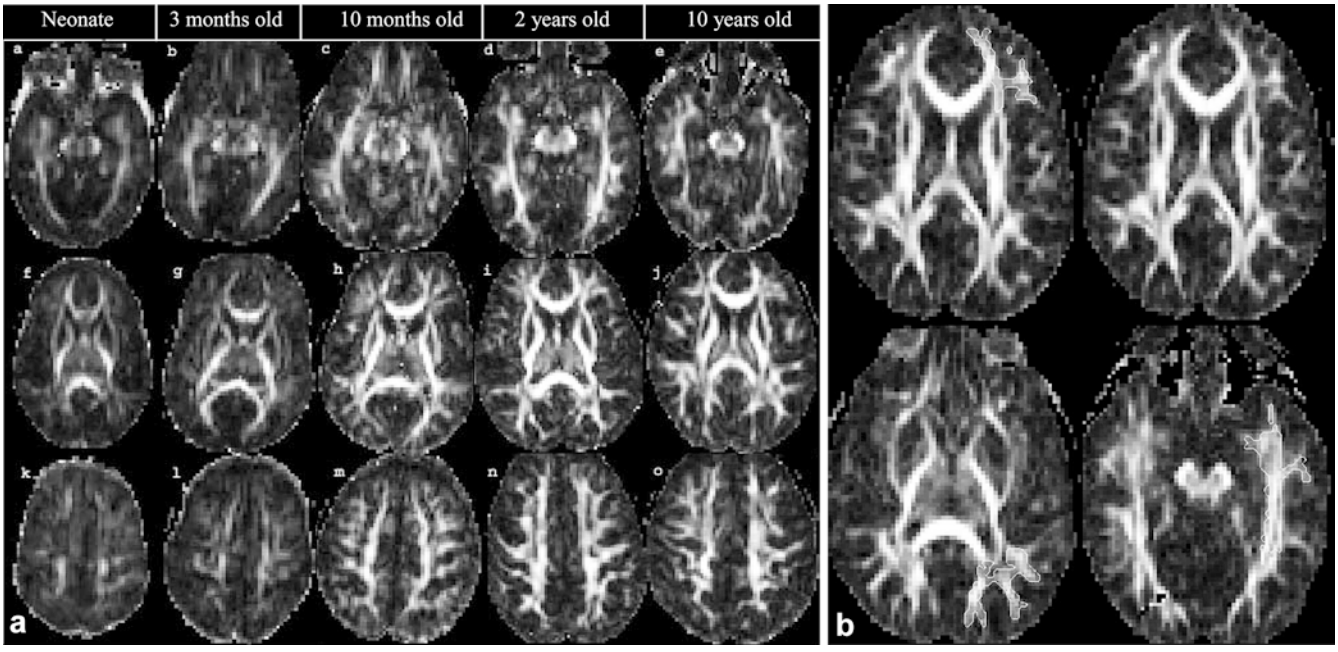


**Fig. 2a, b** Axial FA maps. **a** through the cerebral peduncle and temporal lobes (*a–e*), basal ganglia (*f–j*) and centrum semiovale/corona radiata (*k–o*) in five children, showing the development of FA. **b** Examples of the manually selected regions of interest in the left frontal white matter (*top left*), left side of the genus of the corpus callosum (*top right*), left occipital (*bottom left*), and temporal (*bottom right*) white matter

Myelin also impairs the exchange of water molecules across the cell membrane. As the intracellular structures and cell membrane limit the movement of intracellular water, the relative decrease in extracellular water results in a relative decrease of D' in myelinated white matter. In addition, because of cell structure, the movement of intracellular water is restricted perpendicular to the length of the axon rather than parallel to it, causing a proportional increase in FA (Fig. 2a, b) [8, 11, 12]. Experimental studies have shown that intact membranes are the primary determinant of anisotropic water diffusion in nerve fibres and that myelination only can modulate the degree of anisotropy [26].

We have shown a hierarchy of tissue types, categorising the white matter into commissural, projection and association fibres [27]. This is even more marked when considering FA rather than D'. At birth, the highest FA was seen in the corpus callosum, which belongs to the commissural fibres. The genu and splenium follow a nonidentical but strictly parallel course for FA and D', the splenium consistently showing higher FA and lower D', consistent with an earlier stage of myelination. Both regions reached adult values during the third year of life, with the splenium still showing slightly higher FA, whereas D' values were almost identical. In the corticospinal tracts, which are projection fibres, PLIC and Crus had higher FA than CSO and Pons. The observation that vasogenic oedema preferentially spreads into projection fibres in mild cases and into commissural fibres only in severe cases, suggests that FA may correlate with resistance to spread of fluid, possibly owing to dependence on common histological structural features of white matter, as fibre-packing density, myelination, order and/or directional coherence [27]. The association fibre areas in the deep white matter of frontal, temporal, parietal and occipital lobes had the lowest FA in newborns (Fig. 3a). Despite very different FA of association and commissural fibre areas, their D' are almost identical during whole brain maturation. Adult D' values were reached for all fibre types at approximately the end of the second year (Fig. 3). In deep white matter, the time-course for FA and D' is different. D' values are almost identical during maturation in all four regions but FA was clearly distinct and following a parallel course. TWM and OWM show a clearly higher FA than PWM and FWM at birth and during the entire maturation process. Adult FA of FWM is even lower than in the other three regions, reflecting the fact that myelination of the frontal lobe occurs last. Moreover, there are no early organised myelinated white-matter tracts which produce higher FA values, as in the OWM, i.e., the visual pathways. We observed a small but continued increase in anisotropy and fall in diffusion in FWM until late childhood and adolescence, unlike all other areas, but consistent with previous studies [5], reflecting continued myelination and/or organisation of the FWM and associative pathways well into adolescence. Whether these processes parallel the ongoing acquisition of skills and achievement of cognitive milestones is the subject of further investigation.

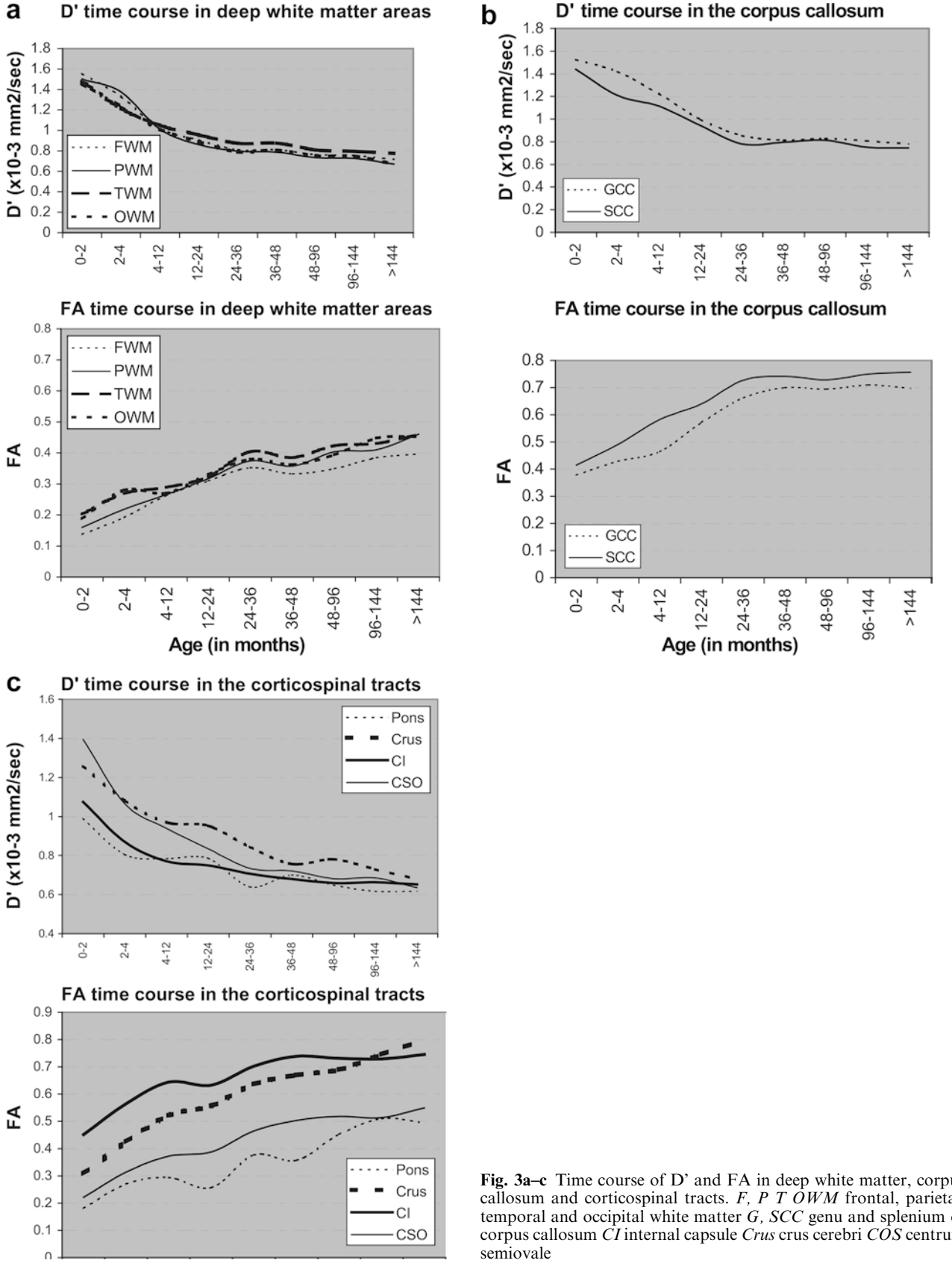


**Fig. 3a–c** Time course of D' and FA in deep white matter, corpus callosum and corticospinal tracts. *F, P T OWM* frontal, parietal, temporal and occipital white matter *G, SCC* genu and splenium of corpus callosum *CI* internal capsule *Crus* crus cerebri *COS* centrum semiovale

We found that monoexponential functions reliably expressed the age-dependency of D' for the commissural (GCC, SCC) and projection fibres (PLIC, Crus), whereas a biexponential function gave the most accurate fitting for deep association fibres (Table 3). Two exceptions are identified: for the projection-fibre areas CSO and Pons a biexponential fit (strong correlation for CSO, weak for Pons) was the best algorithm, probably due to a loss of compactness as the corticospinal tracts fan out in the corona radiata and more intense fibre crossing takes place, especially in the pons.

The fast exponential component of the maturational decline in the magnitude of water diffusion D' might be linked to the decreasing amount of extracellular space or to increasing concentration of intracellular macromolecules [24]. On the other hand, a plausible mechanism for the slow component of D' decay might be an ongoing reduction in the total water content of the brain, which decreases by 14%–18% from birth to adulthood [13]. The monoexponential D' decay of the projectional fibres in the PLIC and the commissural fibres of the corpus callosum might be explained by the densely packed fibre bundles and the small extracellular space (Table 3) There was not as much consistency regarding the best-fit algorithms for FA as with D'. Densely packed projectional fibres, like the PLIC, or commissural fibres like GCC and SCC did maintain a monoexponential rise in FA.

This study provides a normative database of brain white-matter development from neonates to early adolescence. Appreciation of the normal changes in D' and FA with age is important when interpreting DTI, particularly in cases of global ischaemia or white-matter degenerative disease.

## References


1. Basser PJ, Mattiello J, LeBihan D (1994) MR diffusion tensor spectroscopy and imaging. Biophys J 66: 259–267
2. Mori S, van Zijl PC (1995) Diffusion weighting by the trace of the diffusion tensor within a single scan. Magn Reson Med 33: 41–52
3. Baratti C, Barnett AS, Pierpaoli C (1999) Comparative MR imaging study of brain maturation in kittens with T1, T2, and the trace of the diffusion tensor. Radiology 210: 133–142
4. Huppi PS, Maier SE, Peled S, et al (1998) Microstructural development of human newborn cerebral white matter assessed in vivo by diffusion tensor magnetic resonance imaging. Pediatr Res 44: 584–590
5. Klingberg T, Vaidya CJ, Gabrieli JD, et al (1999) Myelination and organization of the frontal white matter in children: a diffusion tensor MRI study. Neuroreport 10: 2817–2821
6. Pierpaoli C, Basser PJ (1996) Toward a quantitative assessment of diffusion anisotropy. Magn Reson Med 36: 893–906
7. Pierpaoli C, Jezzard P, Basser PJ, et al (1996) Diffusion tensor MR imaging of the human brain. Radiology 201: 637–648
8. Nomura Y, Sakuma H, Takeda K, et al (1994) Diffusional anisotropy of the human brain assessed with diffusion-weighted MR: relation with normal brain development and aging. AJNR 15: 231–238
9. Morriss MC, Zimmerman RA, Bilaniuk LT, et al (1999) Changes in brain water diffusion during childhood. Neuroradiology 41: 929–934
10. Prayer D, Barkovich AJ, Kirschner DA, et al (2001) Visualization of nonstructural changes in early white matter development on diffusion-weighted MR images: evidence supporting premyelination anisotropy. AJNR 22: 1572–1576
11. Wimberger DM, Roberts TP, Barkovich AJ, et al (1995) Identification of "premyelination" by diffusion-weighted MRI. J Comput Assist Tomogr 19: 28–33
12. Barkovich AJ (2000) Concepts of myelin and myelination in neuroradiology. AJNR 21: 1099–1109
13. Neil JJ, Shiran SI, McKinstry RC, et al (1998) Normal brain in human newborns: apparent diffusion coefficient and diffusion anisotropy measured by using diffusion tensor MR imaging. Radiology 209: 57–66
14. Basser PJ, Pierpaoli C (1996) Microstructural and physiological features of tissues elucidated by quantitative-diffusion-tensor MRI. J Magn Reson B 111: 209–219
15. Conturo TE, Lori NF, Cull TS, et al (1999) Tracking neuronal fiber pathways in the living human brain. Proc Natl Acad Sci USA 96: 10422–10427
16. Basser PJ, Pajevic S, Pierpaoli C, et al (2000) In vivo fiber tractography using DT-MRI data. Magn Reson Med 44: 625–632
17. Jones DK, Horsfield MA, Simmons A (1999) Optimal strategies for measuring diffusion in anisotropic systems by magnetic resonance imaging. Magn Reson Med 42: 515–525
18. Bastin ME, Armitage PA (2000) On the use of water phantom images to calibrate and correct eddy current induced artefacts in MR diffusion tensor imaging. Magn Reson Imaging 18: 681–687
19. Simpson JH CH (1958) Diffusion and nuclear spin relaxation in water. Phys Rev 111: 1201–1202
20. Mukherjee P, Miller JH, Shimony JS, et al (2001) Normal brain maturation during childhood: developmental trends characterized with diffusion-tensor MR imaging. Radiology 221: 349–358
21. Jezzard P, Barnett AS, Pierpaoli C (1998) Characterization of and correction for eddy current artifacts in echo planar diffusion imaging. Magn Reson Med 39: 801–812
22. Haselgrove JC, Moore JR (1996) Correction for distortion of echo-planar images used to calculate the apparent diffusion coefficient. Magn Reson Med 36: 960–964
23. Papadakis NG, Xing D, Houston GC, et al (1999) A study of rotationally invariant and symmetric indices of diffusion anisotropy. Magn Reson Imaging 17: 881–892

24. Engelbrecht V, Scherer A, Rassek M, et al (2002) Diffusion-weighted MR imaging in the brain in children: findings in the normal brain and in the brain with white matter diseases. Radiology 222: 410–418
25. Tanner SF, Ramenghi LA, Ridgway JP, et al (2000) Quantitative comparison of intrabrain diffusion in adults and preterm and term neonates and infants. Am J Roentgenol 174: 1643–1649
26. Shimony JS, McKinstry RC, Akbudak E, et al (1999) Quantitative diffusion-tensor anisotropy brain MR imaging: normative human data and anatomic analysis. Radiology 212: 770–784
27. Cowley AR (1983) The Dyke Award. Influence of fiber tracts on the CT appearance of cerebral edema: anatomic-pathologic correlation. AJNR 4: 915–925